Impact of the variability of material constitutive models on the thermal response of reinforced concrete walls

Abstract

Purpose – This study examines the effect of temperature-dependent material models for normal-strength and high-strength concrete on the thermal analysis of RC walls.

Design/methodology/approach – The study performs a One-at-a-Time sensitivity analysis to assess the impact of variables defining the constitutive and parametric fire models on the wall's thermal response. Moreover, it extends the sensitivity analysis to variance-based analysis to assess the effect of constitutive model type, fire model type, and constitutive model uncertainty on the RC wall's thermal response variance. The study determines the wall's thermal behaviour reliability considering the different constitutive models and their uncertainty.

Findings – It is found that the impact of the variability in concrete's conductivity is determined by its temperature-dependent model, which differs for normal- and high-strength concrete. Therefore, more testing and improving material modelling are needed. Furthermore, the heating rate of the fire scenario is the dominant factor in deciding fire resistance performance because it is a causal factor for spalling in high-strength concrete walls. And finally the reliability of wall's performance decreased sharply for high-strength concrete walls due to the expected spalling of the concrete and loss of cross-section integrity.

Originality/value – limited studies in the current open literature quantified the impact of constitutive models on the behaviour of reinforced concrete walls. No studies have examined the effect of material models' uncertainty on wall's response reliability under fire. Furthermore, the study's results contribute to the ongoing attempts to shape performance-based structural fire engineering.

Keywords fire, constitutive models, thermal analysis, walls, sensitivity analysis, normal-strength concrete, high-strength concrete

Paper type Research paper

1 Introduction

Following a wide range of research studies on concrete, it was observed that the material properties of High-Strength Concrete (HSC) vary differently with temperature as compared to those of Normal-Strength Concrete (NSC) (Ali, 2002; Castillo and Durrani, n.d.; Kodur, 2008; Mendis, 2003; Ngo *et al.*, 2013; Nguyen *et al.*, 2018; Phan, 2008; Sanjayan, 2011). These research studies among others have concluded that HSC elements are more temperature-sensitive than NSC elements, and failure due to fire exposure will occur earlier for HSC elements. According to the experimental work of concrete members exposed to fire, there are notable differences between the properties of HSC and NSC in terms of the change in their thermal and mechanical properties and the degree of spalling at elevated temperatures, and consequently, loss of cross-section. The most remarkable observation and finding is that HSC has a higher potential for serious spalling due to fire when compared to NSC. The risk of spalling is higher in HSC due to its low permeability and porosity as this retains moisture inside the concrete and increases pore pressure.

There is a broader use of high-strength concrete (HSC) in load-bearing structural elements like walls due to its higher strength and durability and feasible manufacturing. In addition to these walls bearing loads, they will act as fire-separating elements between compartments in modern buildings. Therefore, they must satisfy the fire safety requirements, integrity, insulation and structural adequacy at high temperatures. Despite the growing use of load-bearing HSC walls in buildings, major design codes, including the American Codes, do not cover the behaviour of HSC adequately; and the Eurocode rules were developed using limited research. Furthermore, few investigations are found on HSC walls subjected to fire conditions (e.g. Damian et al., 2000; Mueller and Kurama, 2015; Ngo et al., 2013; Nguyen et al., 2018). The results of the experimental work indicated that the thermal and mechanical analysis of HSC walls differed from the NSC walls. HSC walls experienced moderate to severe spalling under the considered fire scenarios. (Ngo *et al.*, 2013; Nguyen *et al.*, 2018)concluded that the tendency of spalling is higher when the temperature rise of the fire is rapid, and concrete is subjected to a high thermal gradient, such as in hydrocarbon fire.

To assess the performance of HSC walls, better modelling of constitutive material models is needed, including spalling. Several researchers have proposed models to consider concrete spalling in walls, especially high-strength concrete walls. For example, (Nguyen *et al.*, 2018) modelled concrete walls subjected to load and fire, considering the spalling of concrete for HSC walls. To account for spalling, the researchers removed concrete elements that spalled as the exposure time progressed based on the experimental results of their examined walls(Nguyen *et al.*, 2018). (Janssens and Dasgupta, 2020) developed a different approach to model the behaviour of concrete walls exposed to fire loading that resulted in spalling. Part of their approach was defining two concrete material curves: spalling and no-spalling. The average thermal conductivity versus temperature curve provided in the standards was used for no-spalling case. Sharply increasing the concrete thermal conductivity when it exceeded the critical spalling temperature was used for the spalling case.

The study examines the effect of temperature-dependent material models for normal-strength and high-strength concrete on the thermal analysis of RC walls. It considers the uncertainties in material models and fire scenarios due to the different testing procedures and performs a One-at-a-Time sensitivity analysis to assess the impact of variables defining the constitutive and parametric fire models on the wall's thermal response. Moreover, it extends the sensitivity analysis to variance-based analysis to assess the effect of constitutive model type, fire model type, and constitutive model uncertainty on the RC wall's thermal response variance. The study determines the wall's reliability using its thermal performance, considering the different constitutive models and their uncertainty. The results contribute to the ongoing attempts to shape performance-based structural fire engineering.

2 Sensitivity analysis and the thermal performance assessment procedure

One-at-a-Time (OAT) approach was used to measure the sensitivity of the wall's thermal response to the fire's input variables and constitutive models. For applying OAT sensitivity analysis, a base case for the parametric fire and constitutive models was selected to obtain a reference response for the wall behaviour.

The OAT approach builds on the notion that fire duration and severity in a fully developed fire depend on the amount of ventilation, nature, distribution, and fuel quality. A double or triple-glazed system in a modern building may not break as fast as single panels of ordinary glass. Moreover, the glazed external openings' characteristics, orientation, and dimensions are selected based on architectural aspects that cannot be controlled. Due to the aforementioned, uncertainties associated with glass breakage and fall-out glass may lead to fuel-controlled or ventilation-controlled fires.

To cover all possibilities of ventilation, a series of parametric temperature-time curves were developed, in which the opening factor varied from 0.02 $m^{1/2}$ -0.2 $m^{1/2}$, following the limitations documented by EC1(Eurocode 1, 2005). The thermal inertia of the concrete was assumed to be 1680 $Ws^{1/2}/m^2K$. The examined building category is assumed to be a dwelling, and the mean value for fuel load for dwellings is 780 $MJ/m^{2,}$ according to EC1. The developed compartment temperatures for different opening factors. It can be seen from Fig. 1 that opening factors lying between

0.08 and 0.2 $m^{1/2}$ produced a relatively short fuel-controlled fire. The decrease in opening factor to below 0.08 $m^{1/2}$ resulted in a fire controlled by ventilation. The limiting design fire scenario between the ventilation and fuel-controlled fire curves was used as the parametric fire model for the base case. The median values were used for temperature-dependent models for normal-strength and high-strength concrete properties; thus, they were used for the base case.

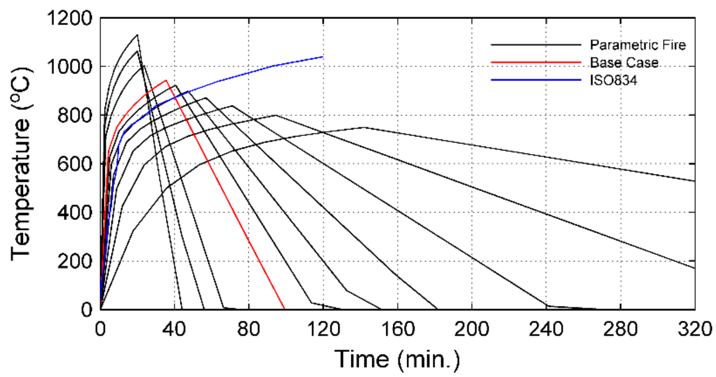

Fig. 1. Parametric fire models considering different opening factors

The probabilistic models were used to run the OAT analysis and evaluate the impact of the input variables' variability. The analysis was run for the *16th* and *84th* fractiles of their distribution. The variability in y (output variable) due to input variability was calculated as follows

$$\Delta_y = 100 \cdot {(y_{ij} - y_{bc})}/{y_{bc}} \ \% \tag{1}$$

Where y_{ij} is the value of the output parameter computed for the variation of the i^{th} input variable to the j^{th} fractile, y_{bc} corresponds to the value of the output parameter estimated for the base-case model.

In the case of a RC wall exposed to fire loading, three criteria (limit states) for its failure can be expected, (1) stability criterion: the capability of carrying applied loads during fire exposure; (2) insulation criterion: the capability of maintaining temperature on an unexposed side below the temperature of ignition; and (3) integrity criterion: the capability of providing compartmentation from fire via preventing crack development. The thermal response parameter for the first two criteria may be the steel rebars' and the unexposed surface's temperatures, respectively. The rebars were assumed to have the same temperature as the adjacent concrete, as steel has a much higher thermal diffusivity than concrete. Furthermore, the times to reach the maximum temperature for rebars and the unexposed surface were considered in the analysis as a performance indicator.

Moreover, it is essential to quantify the effect of constitutive model choice, fire model choice, and randomness in the material properties variables on the variance of thermal response since this is important to assess the reliability of the analysis results. The global variance-based method by Sobol (Saltelli et al. 2008) is generally used for such a purpose. It is based on the decomposition of the total unconditional variance (as a measure of the uncertainty) of the model's output *V(Y)*. The total unconditional model variance *V(Y)* (Andrea Saltelli, Marco Ratto, Terry Andres, Francesca Campolongo, Jessica Cariboni, Debora Gatelli, Michaela Saisana, 2008) is represented by Eq. 2.

$$V(Y) = V_{X_{\sim i}}\left(E_{X_i}(Y|X_{\sim i})\right) + E_{X_{\sim i}}\left(V_{X_i}(Y|X_{\sim i})\right) \tag{2}$$

The first term is the variance explained conditioned on input parameter x_i (which indicates the first-order effect), and the second term is the remaining variance. The inner operator of the second term is the variance of *Y* taken over all possible values of the input matrix **X** except for one x_i. Moreover, the outer expectation is taken over all possible values of x_i. The total effects sensitivity index (Andrea Saltelli, Marco Ratto, Terry Andres, Francesca Campolongo, Jessica Cariboni, Debora Gatelli, Michaela Saisana, 2008) that determines the effect of the ith input variable and its interactions is expressed by Eq. 3 as:

$$S_{T_i} = \frac{E_{X_{\sim i}}\left(V_{X_i}(Y|X_{\sim i})\right)}{V(Y)} \tag{3}$$

Total sensitivity indices can be calculated using the elementary effects approach (similar to OAT setting with repetitions in its application) as long as enough repetitions (*r*) are performed (Saltelli et al. 2008). For this purpose, the estimation of $E_{X_{\sim i}}\left(V_{X_i}(Y|X_{\sim i})\right)$ is expressed by Eq. 4 (Campolongo *et al.*, 2011)

$$E_{X_{\sim i}}\left(V_{X_i}(Y|X_{\sim i})\right) = \frac{1}{2r}\sum_{j=1}^{r}\left(y\left(a_1^j, a_2^j, \dots, a_k^j\right) - y\left(a_1^j, a_2^j, \dots, b_i^j, \dots, a_k^j\right)\right)^2 \tag{4}$$

where $y(x_i^A x_{\sim i}^A)$ is the output considering only variables of base vector **A**, $y(x_i^B x_{\sim i}^A)$ is the output considering the variables of base vector **A** except for x_i chosen from auxiliary vector **B**. **A** and **B** are two different *k*-dimensional random vectors for the *k* input variables considered in the sensitivity analysis.

Reliability Analysis

This analysis examines the reliability of the thermal performance of the concrete walls constructed from normal-strength and high-strength concrete. In general, a failure criterion is defined in terms of a limit state function defined for the target performance measure, e.g., for the thermal analysis $g(X) = R - F$, where R is the actual thermal response (resistance) of the wall, and F is the thermal-failure criteria.

The failure probability is expressed in Eq. 5 and defined as the probability that the limit state function attains non-positive values

$$P_f = Prob[g(x_1, x_1, \dots, x_n) \leq 0] = \int_{g(X)\leq 0} \dots \int f_X(X)dX \tag{5}$$

The computational challenge is in determining the integral. This integral is determined using Monte Carlo simulation. The reliability analysis accounts for the uncertainties of the variables defining the characteristic fire model and the variables defining the heat transfer mechanisms. In Monte Carlo simulations, a random value is selected for each input variable based on the developed probabilistic models, and a failure criterion is assigned for a response function. The probability of failure (P_f) is calculated using $P_f = {}^{n_f}/_{n}$.

Where, n_f is the number of samples exceeding the failure criterion, and n is the total number of run samples. The model is run repeatedly in a Monte Carlo simulation until the value of the outputs converges. The result of the Monte Carlo simulation is used to determine the reliability index (β), which indicates the margin of safety for the structural element's performance. Assuming a Gaussian response (Novak A. S., 2013), then

$$\beta = {}^{\bar{R} - \bar{F}}\Big/_{\sqrt{\sigma_R^2 + \sigma_F^2}} \tag{6}$$

where $\bar{R}$ and $\bar{F}$ are the mean value for resistance and failure limit, consequently, and σ_R^2 and σ_F^2 are the variance of resistance and failure limit. If the limit state function is not Gaussian, Eq. 6 only approximates the reliability index (β). In case the limit state function follows a lognormal distribution, Eq. 7, proposed by Withiam et al. (1998), will be used to calculate □

$$\beta = {}^{ln[\bar{R}/\bar{F}\sqrt{(1+COV_F^2)/(1+COV_R^2)}]}\Big/_{\sqrt{ln[(1+COV_F^2)(1+COV_R^2)]}} \tag{7}$$

where COV_R coefficient of variation for the resistance and COV_F coefficient of variation for the failure limit.

3 Numerical Model of Reinforced Concrete Wall

3.1 Finite element model

Finite element analysis is usually used to evaluate the thermal behaviour of structural elements exposed to different fire scenarios (Hawileh and Kodur, 2018). The developed model herein is based on a simply supported wall specimen tested by (Ngo *et al.*, 2013). The tested wall specimen's total height, width, and thickness were 2400, 1000, and 150 mm, respectively. The specimens of normal-weight concrete (NSC wall) and high-strength concrete (HSC wall) were tested under a fire scenario ISO834. The walls reinforcement was two layers in vertical (N16 at 300mm) and horizontal (N14 at 300mm) directions, with a clear cover of 25mm. The concrete mix design and details of the tested walls considered in this study are shown in Table 1.

Table 1. Concrete mixture constituents and properties of tested walls

Component	NSC-3	HSC-1
Cement, kg	320	600
Aggregate (coarse aggregate), kg	828 (size: 10 to 20 mm)	1029 (size: 5 to 10 mm)
Sand, kg	925	586
Water-binder ratio	0.59	0.235
28-day compressive strength, Mpa	31.8	81.8
Test day compressive strength, Mpa	35.6	87.6
Initial moisture content, %	8.4	5.7

The FE model for the longitudinal strip of the wall specimen is developed using ANSYS version 19 (ANSYS 2019). A FE model of a strip of the concrete wall is adequate to simulate the behaviour of the wall due to symmetry in the geometry, materials, fire loading, and thermal boundary conditions of the tested wall, Fig. 2. The use of a strip model to simulate the wall behaviour leads to a significant reduction in computational time and effort. Thermal symmetry must be achieved; no heat will flow across the symmetrical plane. Therefore, no boundary conditions nor constraints were defined on the symmetry plane. The element types used to discretise the concrete core and steel rebars were 3D brick SOLID70 and LINK33, respectively. These elements can conduct heat throughout the wall's model due to transient heating resulting from fire applied at the exposed surface of the wall. The 3D brick SOLID70 element, used for thermal discretisation, has eight nodes. Each node of the SOLID70 element has one degree of freedom (*DOF*), namely temperature. Two nodes with a temperature DOF define the 3D spar uniaxial thermal LINK33 element. The SOLID70 and LINK33 element types can be used in steady-state or transient thermal analyses.

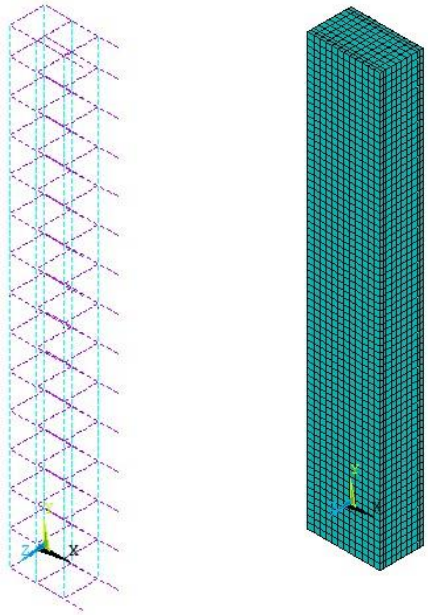

Fig. 2. Schematic of the modelled reinforced concrete wall and steel rebars

The wall is exposed from one side to the ISO834 standard fire scenario (Ngo *et al.*, 2013). Transient thermal analysis is performed for which conduction is the mechanism to describe the heat flow through the solid media, and convection and radiation are the primary mechanisms for net heat flux applied on the boundary surface.

The experimental results of the thermal analysis of NSC and HSC walls showed that their thermal behaviour differed. The HSC wall suffered more from early concrete spalling. Therefore, HSC wall was exposed to increased temperatures within its section much earlier than NSC. Spalling occurred within 25 minutes of the wall being exposed to fire, at which the temperature at the spalling point was between 200ºC to 400ºC (Ngo *et al.*, 2013). The FEM model of the wall was developed depending on the experimental observation of concrete spalling and using developed approach by (Janssens and Dasgupta, 2020). Thus, two different curves for the thermal conductivity of concrete were developed to investigate the no-spalling and spalling cases, respectively. The average thermal conductivity versus temperature curve proposed in Eurocode 2, part 1-2 was used for concrete not assumed to spall.

The spalling case was simulated by rapidly increasing the thermal conductivity of the concrete when it exceeds the critical temperature at which spalling is assumed to occur. Thus, instead of physically removing each spalled layer, the material is suddenly considered to have very low to negligible thermal resistance (Janssens and Dasgupta, 2020). The thermal conductivity of concrete above the spalling temperature is assumed to increase sharply. For the examined wall, it was observed that spalling temperature of the concrete was around 340ºC, (Ngo *et al.*, 2013). In this work, the thermal conductivity for HSC concrete beyond the assumed spalling temperature was sharply increased using an inverse calibration procedure based on the temperature profiles of the steel rebars and unexposed surface, Fig. 3. The spalling temperature was assumed around 300°C as Spalling is attributed to the build-up of pore pressure during heating. HSC is more vulnerable to this pressure due to its low permeability and high density. As high vapour cannot escape, then pressure will reach saturation vapour pressure, which is about 8MPa at around 300°C. This internal pressure exceeds the tensile strength of HSC, which is about 5MPa, and hence, spalling occur (Kodur and Mcgrath, 2003).

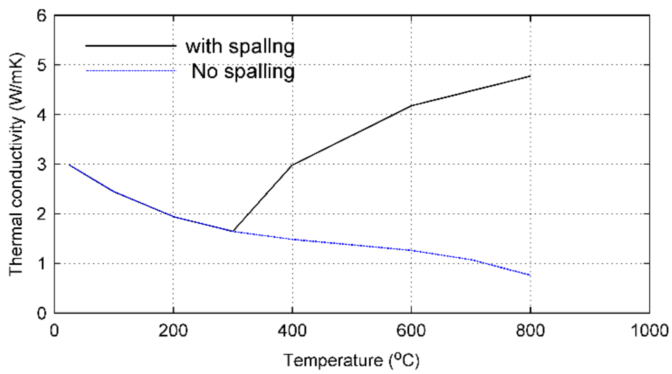

Fig. 3. Thermal conductivity considering the spalling of the concrete of HSC

Fig. 4 and Fig. 5. show the measured and numerical model-predicted temperature profiles. There is a reasonable agreement between the experimental and numerical model analysis results for normal-strength and high-strength concrete, which means that the modelling uncertainty is somewhat controlled. The spalling temperature for HSC wall depends on water moisture, which is not considered as a variable in this study. Thus, spalling temperature is accepted for further analysis in this study.

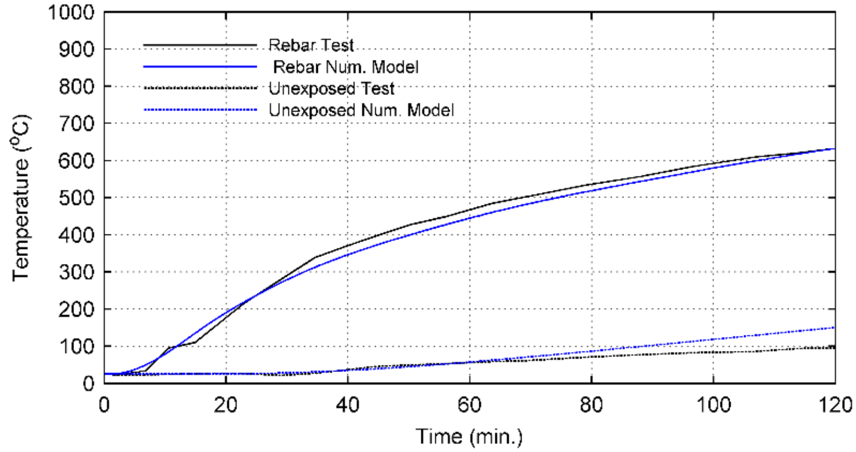

Fig. 4. The progression of thermal response of NSC wall with time

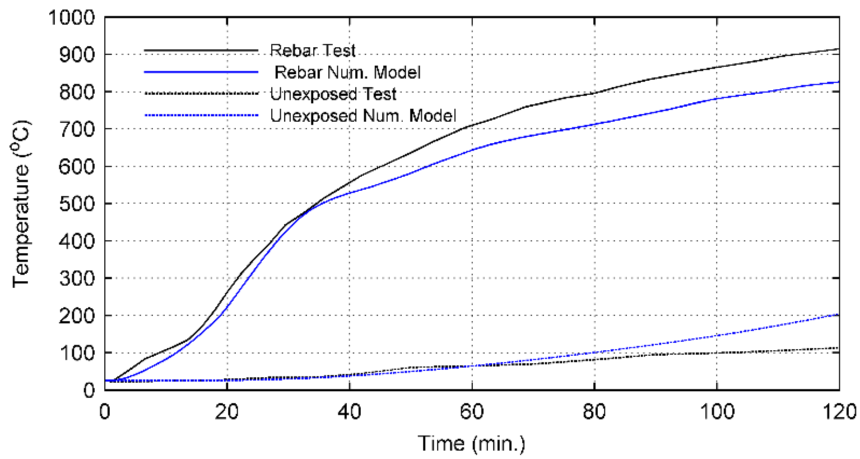

Fig. 5. The progression of thermal response of HSC wall with time

3.2 Material Models

The materials examined in this study are normal-strength concrete and high-strength concrete. In a study by (Karaki *et al.*, 2021), the authors conducted a screening sensitivity analysis and concluded that the thermal properties of steel do not affect the thermal response of RC members exposed to fire loading since their volume is relatively small compared to the surrounding concrete elements. However, their effect would be significant on the mechanical response of the concrete member. Therefore, only the thermal properties of concrete are considered in this study.

The probabilistic models for the properties of normal-strength and high-strength were developed by (Karaki and Naser, 2022). The developed probabilistic material models are temperature-dependent continuous functions for a set of parameters defining fitted probability distribution functions. Temperature-dependent distribution parameters were evaluated for the analysis, and probability distribution functions were created. A user-input fractile was utilised to obtain a point on the created probability distribution function and used in the thermal analysis of the structural element. The following sections describe the constitutive thermal material models.

Thermal Conductivity

The regression model for the parameters defining the probabilistic model for the conductivity of normal-strength concrete is presented in Table 2 and Fig. 6. Overall, the scatter in the data points of the thermal conductivity is higher for normal-strength concrete, which affected the regression quality.

Table 2. Models for the variables defining the probabilistic models for the thermal conductivity of concrete

Type	Dist.	Model	R^2
NSC	Weibull	$A = 1.7106 - 1.5246 \cdot T_{std} + 0.5222 \cdot T_{std}^2$	0.98
	A-scale factor	$B = 4.8809 + 3.6512 \cdot T_{std} - 6.8362 \cdot T_{std}^2$	0.65
	B-shape factor		
HSC	Normal	$\mu = 2.9885 - 6.5231 \cdot T_{std} + 9.5980 \cdot T_{std}^2 - 5.3069 \cdot T_{std}^3$	0.98
	μ-mean	$\sigma = 0.3689 - 0.5716 \cdot T_{std} + 0.4185 \cdot T_{std}^2$	0.88
	σ-standard deviation		

The lower the water content and the denser the microstructure, the higher the conductivity of the hardened concrete; therefore, the conductivity at ambient temperature is higher for high-strength concrete, Fig. 6. In addition, the experimental data showed that the decrease of the thermal conductivity with temperature was higher for high-strength concrete than normal-strength concrete. This may be linked to the complex behaviour of HSC related to heat-induced transformations and transport of capillary-bond and chemically-bond water, which are more pronounced in the temperature range 25ºC to about 400ºC (Phan and Carino, 1998). The developed models captured these observations, as shown in Fig. 6.

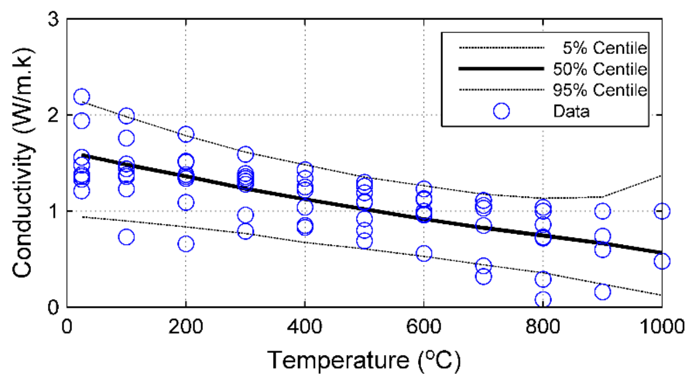

(a) for NSC

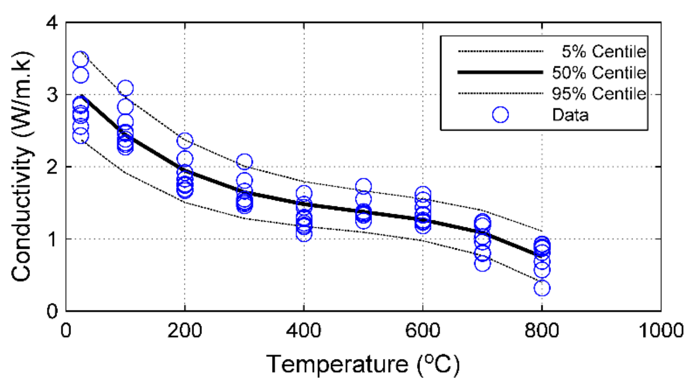

(b) for HSC

Fig. 6. Probabilistic models for the thermal conductivity of concrete

Specific Heat

The developed probabilistic models for the specific heat of concrete are presented in Table 3. The coefficient of determination for the standard deviation of lognormal distribution used in the probabilistic model for the specific heat of normal-strength concrete was low. This is due to the sudden sharp increase in the specific heat at 700ºC stemming from exothermic reactions at the microstructure level often captured by some material models. The developed model predicts a slight rise at 700°C and captures a decrease in specific heat above this temperature. However, fire codes such as Eurocode 2 and the probabilistic model do not capture this sudden increase (see Fig. 7).

Table 3. Models for the variables defining the probabilistic models for the specific heat of concrete

Type	Dist.	Model	R^2
NSC	LogNorm. μ-mean	$\mu = 6.0345 + 1.1756 \cdot T_{std} - 0.2906 \cdot T_{std}^2$	0.93
	σ-standard deviation	$\sigma = 0.3894 + 0.5245 \cdot T_{std} - 0.6485 \cdot T_{std}^2$	0.15
HSC	LogNorm μ-mean	$\mu = 3.4580 - 15.7711 \cdot T_{std} + 25.9841 \cdot T_{std}^2 - 13.1054 \cdot T_{std}^3$	0.85
	σ-standard deviation.	$\sigma = 0.1087 - 0.3441 \cdot T_{std} + 0.5616 \cdot T_{std}^2$	0.95

The experimental data for normal-strength concrete and high-strength concrete showed that the specific heat increases with temperature. For normal-strength concrete, a sharp rise was observed at 700°C, as explained earlier; and for high-strength concrete, rises and drops were marked at multiple temperatures; a rise was noticed at 100°C, a reduction was seen at 400°C (decrease), and a sharp rise was noticed at 700°C (see Fig. 7). Naus (2010) (Naus, 2010) reviewed concrete behaviour and documented that the vaporisation of free water happens at about 100°C, the dissociation of $Ca(OH)^2$ happens at about 400°C - 500°C, and the alpha-beta quartz transformation in some aggregates happens at high temperatures. These may explain these rises and drops in the specific heat values. The behaviour, in general, was depicted in the developed probabilistic models, as noted in Fig. 7.

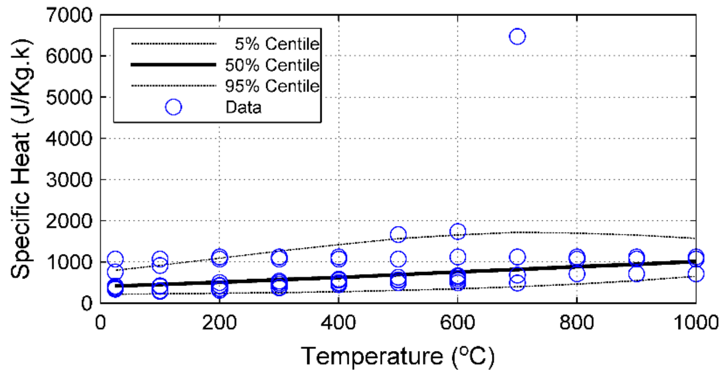

(a) for NSC

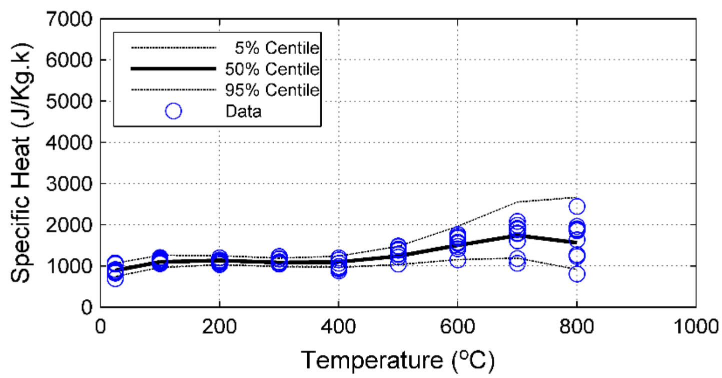

(b) HSC

Fig. 7. Probabilistic models for the specific heat of concrete

3.3 Fire Models

The tendency of spalling is high when the concrete is subjected to a high thermal gradient. Therefore, it is essential to model a fire scenario where its variables can be examined to identify their effect on the response of NSC and HSC walls. Fire scenarios for a fully developed fire were modelled based on input variables such as fuel load density, ventilation size, the contribution of fire protection systems, boundary material properties, floor and total compartment areas. The EC1 (2002) parametric fire method produced a set of temperature-time curves. The analytical equation given in EC1 to calculate the fire temperature is given by Eq. (8):

$$T_g = 1325[1 - 0.324\, exp\, exp\, (-0.2t^*) \; - 0.204\, exp\, exp\, (-1.7t^*) \; - 0.472\, exp\, exp\, (-19t^*)\,]\; (°C)$$

(8.a)

$$t^* = t \cdot \Gamma(h) \tag{8.b}$$

where t is the time in (h), Γ is given as $\Gamma = \frac{\left[\frac{O}{b}\right]^2}{\left(\frac{0.04}{1160}\right)^2}$, where b is the thermal inertia of the enclosure boundary ($J/m^2s^{1/2}K$), and O is the opening factor of the fire compartment ($m^{1/2}$), representing the characteristics of vertical openings in the compartment.

The maximum temperature occurs at t^*_{max} which is calculated as in Eq. 9,

$$t_{max} = max\left[\left(0.2 \cdot 10^{-3} \cdot \frac{q_{t,d}}{O}\right); t_{lim}\right](h) \tag{9}$$

Assuming a medium fire rate, the limiting temperature t_{lim} is taken as 20 minutes. $q_{t,d}$ is the design value of the fire load density related to the total surface area A_t of the enclosure (MJ/m^2), and $q_{f,d}$ is the design value of the fire load density related to the surface area A_f of the floor (MJ/m^2).

$$q_{t,d} = q_{f,d} \cdot \frac{A_f}{A_t} \tag{10}$$

The cooling phase of fire starts after t_{max}, and the temperature-time curve during this phase depends on whether the fire is fuel-controlled or ventilation controlled. These curves are described in EC1, and t_{max} is used to categorise the fire as fuel- or ventilation-controlled. If t_{max} is controlled by t_{lim} then the fire is fuel-controlled, and if $(0.2 \cdot 10^{-3} \cdot q_{t,d}/O)$ controls t_{max} then the fire is ventilation-controlled.

The design value of the fire $q_{f,d}$ is defined as

$$q_{f,d} = q_{f,k} \cdot m \cdot \delta_{q1} \cdot \delta_{q2} \cdot \delta_n \tag{11}$$

where m is the combustion factor taken as 0.8, δ_{q1} is a factor taking into account the fire activation risk due to the size of the compartment taken as 1, δ_{q2} is a factor taking into account the fire activation risk due to the type of occupancy taken as 1.5, and δ_n is a factor taking into account the different active firefighting measures, e.g. detection systems or sprinkler systems among others; it is also referred to as Firefighting measures index (FFMi) as in Heidari et al. (2019). The value $q_{f,k}$ is the characteristic fire load density per unit floor area (MJ/m^2), EC1 gives typical values classified according to the occupancy.

Table 4 presents the variables of the fire model considered in the sensitivity and reliability analyses. Their probabilistic values are also shown in Table 4. The input variables and fire models are created through a MATLAB code that ran ANSYS and applied the developed fire model.

Table 4. Parameters defining the probabilistic model of the characteristic fire

Parameter	**Probabilistic values**	**Notes**	**Reference**
Characteristic fuel load density (q_{fk})	Mean =780MJ/m^2, coefficient of variance =0.3, Gumbel distribution	The value corresponds to the fuel load density of dwellings following EC1 with a mean value of 780MJ/m^2 and 80th percentile of 980MJ/m^2.	EC1
FireFighting Measures Index accounts for the different active firefighting measures (FFMi)	Discrete values are calculated for FFMi, range [0.148-3.37]	The range values cover the possible firefighting measures representing sprinklers, auto detections, safe access routes, and firefighting devices.	EC1
Opening factor (O)	Uniform distribution [0.02-0.2]	Range taken following the limits assigned in EC1. This accounts for uncertainty in the glass breakage and falling out	EC1
Thermal inertia (b)	Uniform distribution [1150-2200]	Range taken to represent the extent of concrete thermal conductivities, specific heats and densities for normal-weight concrete.	----
A_f/A_t	Uniform distribution [0.18-0.35]	Assumed range for the possibilities of the floor area in relation to the enclosure area	----

4 Impact of the Constitutive Models

The impact of constitutive models on the thermal response along the exposure time and the wall's depth was examined. OAT sensitivity analysis was conducted for the effects of the variability in constitutive and fire models. Moreover, a variance-based analysis is conducted to assess the impact of constitutive model choice, fire scenario choice, and variability in material properties on the variance of wall's thermal response at different depths. The effect of the constitutive model parameters on the reliability of the thermal performance of concrete walls was examined.

4.1 Thermal response of RC wall

For the wall examined and modelled in section 3, the temperatures were documented for different wall layers along its depth. Fig. 8 presents the temperature profile along the depth of the wall at a time instant (time to reach maximum temperature). It can be noticed that the effect of the constitutive material model type on the thermal response is higher at the layers near the exposed surface and gets lower at the layers far away from the exposed surface. This is explained by the earlier occurrence of spalling in HSC, which is verified by the experimental results. The conventional models offered by the standards for temperature-dependent material properties may be inadequate to describe a realistic thermal profile of the wall's layers. These thermal profiles are used to identify the percentage of loss in the wall’s cross-section and the loss in the mechanical material properties of the remaining cross section. As time progresses, the difference between the thermal profile considering a wall built from normal-strength concrete and a wall made from high-strength concrete increases and becomes noticeable, as in Fig. 4 and Fig. 5.

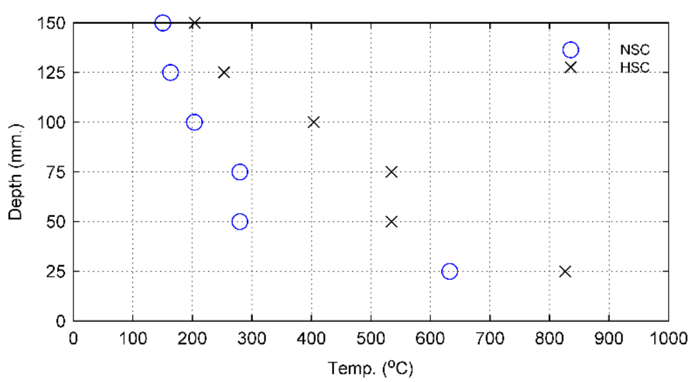

Fig. 8. Temperature distribution along the thickness of the NSC and HSC walls

4.2 OAT sensitivity analysis

The probabilistic models for the variables of parametric fire and material models were created. The one-at-time sensitivity analysis is performed as explained in section 2.0. The difference in the response is determined using the base-case models for fire and material. Fig. 9 examines the impact of fire model parameters on wall's unexposed surface temperatures for normal-strength and high-strength concrete. It can be seen that the variability of firefighting measures, opening factor and fuel load density influences the thermal response of unexposed surface. This trend is actual for NSC and HSC walls as these fire scenario variables affect the duration of exposure and consequently, the temperatures of layers situated away from the exposed surface. In general, the temperatures of these layers are below the assumed spalling temperature, which means that the variability of the fire model affect both walls similarly, which is observed in Fig. 9.

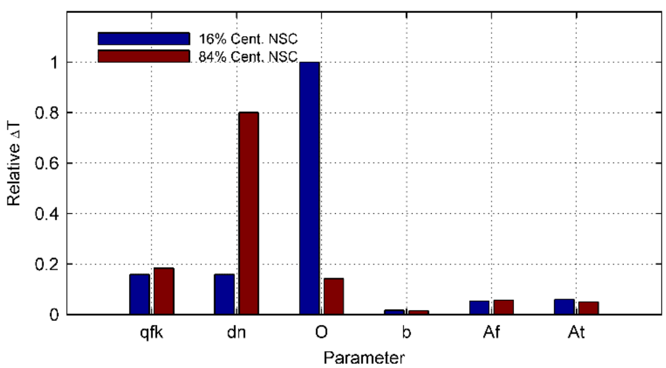

a. Unexposed surface (NCS-Wall)

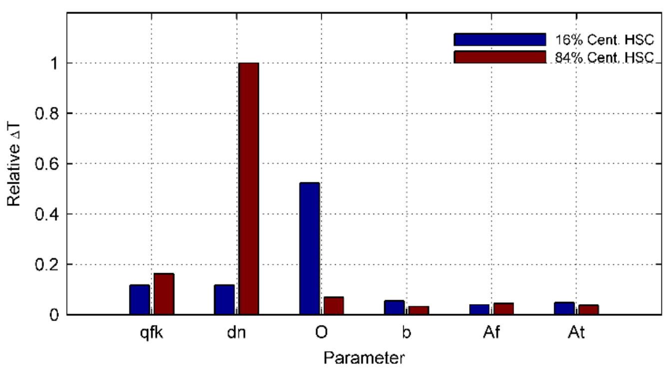

b. Unexposed surface (HCS-Wall)

Fig. 9. OAT sensitivity analysis of material type on impact of fire model parameters on unexposed surface temperatures

Studying the thermal response of steel rebar (see Fig. 10), a similar observation is made regarding the significant effect of variability in fuel load, firefighting measures, and opening factors on thermal response. However, for the HSC wall, the impact of the variation of these variables and concrete thermal capacity on the rebar temperature is more significant. The combination of opening factor and concrete thermal capacity affects the heating rate, and consequently the spalling of concrete. This finding is supported by the experimental work relating the heating rate to the early occurrence of spalling in HSC (Ngo *et al.*, 2013; Nguyen *et al.*, 2018).

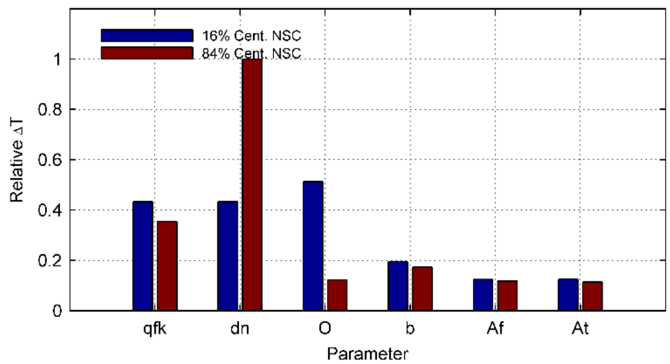

a. Steel rebars (NCS-Wall)

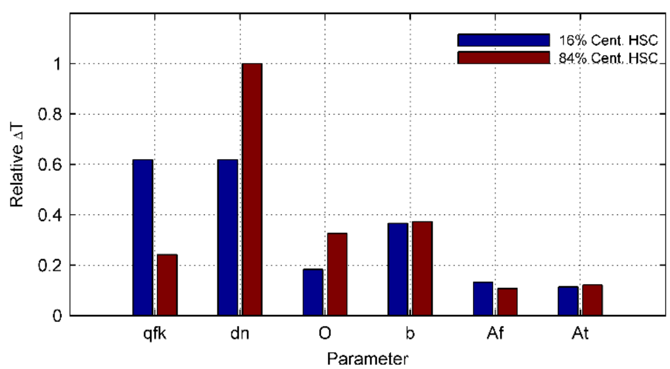

b. Steel rebars (HCS-Wall)

Fig. 10. OAT sensitivity analysis of material type on impact of fire model parameters on steel rebars temperatures

The following analysis investigated the effect of material model parameters variability, thermal conductivity and specific heat capacity, on the thermal response. The thermal response of unexposed surface over the time of fire exposure was examined in Fig. 11 and Fig. 12 presenting the results of 16^{th} and 84^{th} variations in material properties. The impact of the variability of thermal conductivity was influenced by the temperature-dependent rate of decrease in the property and by the scatter of its experimental values. The latter is higher for NSC, evident in its higher impact on unexposed surface temperatures. However, the former impact is clear at the early time of exposure as the rate of decrease is steeper for HSC up to 200ºC. The decreasing rate affects heating of exposed layers of concrete which is transferred to the inner layers at the early stages of fire exposure, this explains the impact of variability of HSC on thermal response of unexposed layers within early periods of exposure. The effect of material type and specific heat's variability on the unexposed surface's thermal response seems the same as the influence of thermal conductivity. In general, it can be said that the variation in experimental data defining the material models significantly impacts reliability of thermal response even for the well-documented normal-strength concrete.

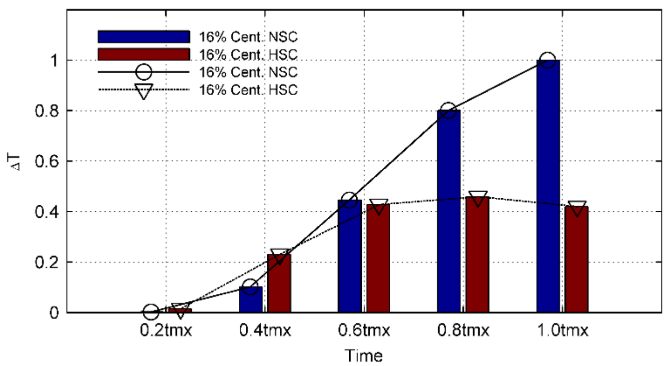

a. Thermal conductivity impact for 16th centile

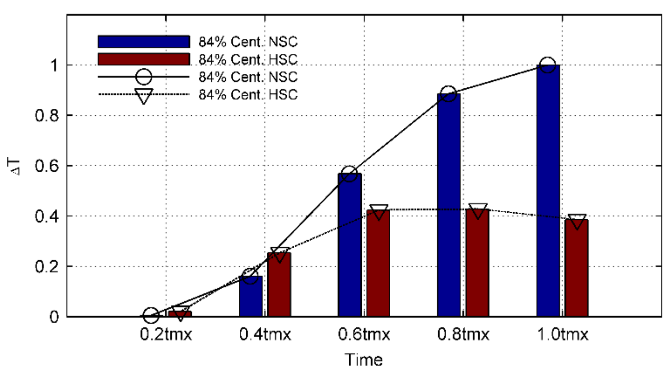

b. Thermal conductivity impact for 84th centile

Fig. 11. Thermal conductivity impact over time for temperatures of unexposed surface of the wall

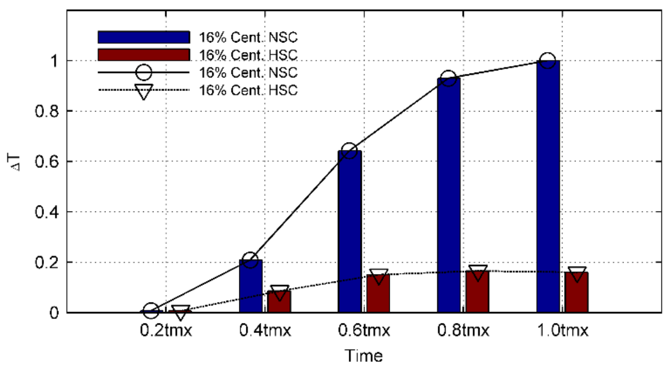

a. Specific heat impact for 16th centile

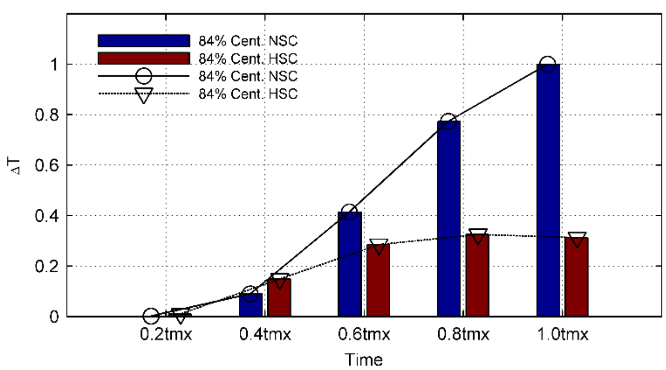

b. Specific heat impact for 84th centile

Fig. 12. Specific heat over time for temperatures of the unexposed surface of the wall

As been discussed earlier, the rate of decrease in the thermal conductivity for HSC is much higher than that of NSC below 400°C temperatures. Therefore, it can be seen in Fig. 13 that for high-strength concrete, the impact of variability in conductivity decreases rapidly and then it has no effect as the concrete already spalled. Furthermore, the variability in conductivity of NSC has a significant effect on the rebar temperatures, which affects the reliability of the thermal response and wall's fire resistance.

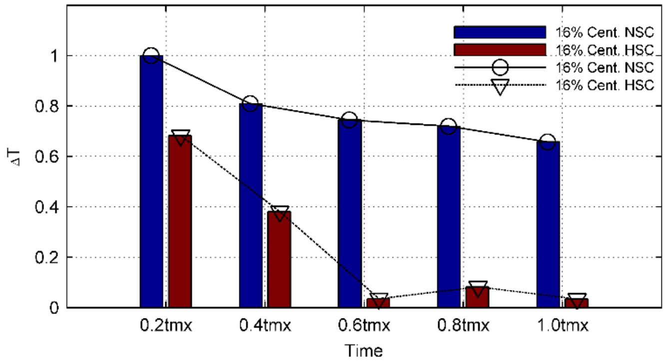

a. Thermal conductivity impact for 16th centile

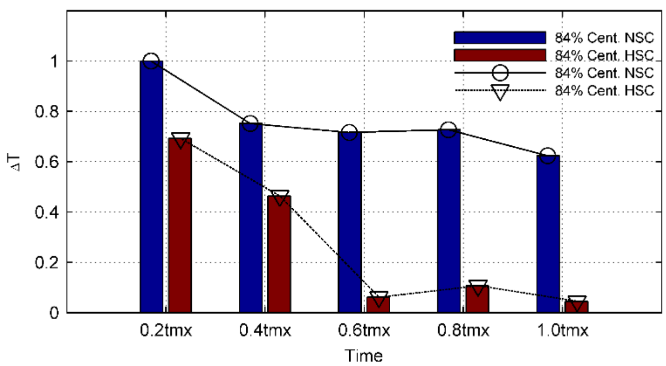

b. Thermal conductivity impact for 84th centile

Fig. 13. Thermal conductivity impact over time for steel rebar temperature

Fig. 14 shows the effect of specific heat capacity on the thermal response of rebars for a wall constructed from normal-strength concrete and high-strength concrete over exposure time. The scatter of the experimental results dominates the impact of variability, for NSC more experimental data is available compared to HSC, and this should encourage more experimental work on the behaviour of HSC with and without spalling remedies to quantify the uncertainty in the constitutive models and consequently performance measures.

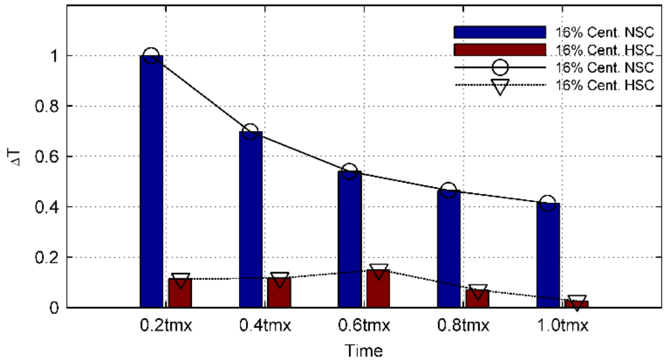

a. Specific heat capacity impact for 16th centile

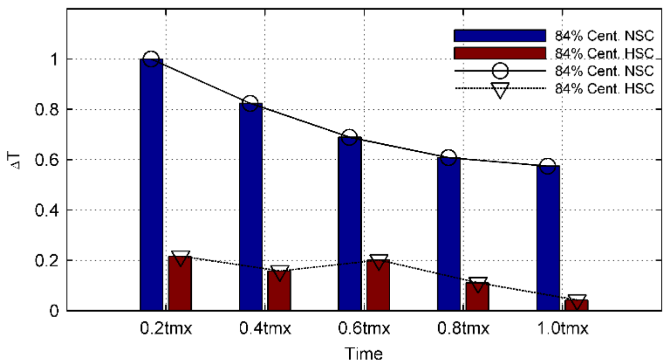

b. Specific heat capacity impact for 84th centile

Fig. 14. Specific heat capacity impact over time for steel rebar temperature

As open literature on experimental work discussed the effect of fire scenario and material type on fire-resistance of walls, the OTA approach was extended to run a variance-based sensitivity analysis, which was used to examine the effect of material type choice, fire scenario choice, and uncertainty in material model on the thermal response as a performance indicator. The median value of developed probabilistic models was used for the material model choice; NSC or HSC. The ISO834 and parametric fire models were used as the fire scenario choices. For the results to be comparable, the chosen parametric fire model has the same duration as the ISO834 fire, and both fire curves had similar maximum temperatures. The variability in the constitutive material models was retrieved from the developed probabilistic models. Table 5 shows the modelling of samples used in the sensitivity analysis; a similar approach is used by Karaki et al. 2021. 500 tests (repetitions) were performed in this analysis, and 2500 simulations were run.

The sensitivity indices were calculated and presented in Table 6 and Table 7. The fire rate and heating rate significantly influence the wall's thermal response, especially for the response of steel rebar, which is consistent with the experimental work (Ngo *et al.*, 2013; Nguyen *et al.*, 2018)as spalling is more probable in HSC walls. Moreover, it is noticed that the material type and its variability significantly influence the thermal response of unexposed surfaces, and this effect is more substantial as the exposure time gets longer. This is expected as the concrete at these layers did not spall and as material models are different, they are expected to affect wall's thermal response. For the steel rebars, the effect of material was noticed at the first stages of fire exposure before the occurrence of spalling in HSC walls as then the heating rate of fire scenario becomes the dominant factor in determining the performance.

Table 5. Mapping of the discrete input variables for sensitivity analysis

Model Indicator	**1**	**2**
Constitutive models types	NSC	HSC
Quantile Range	$0 < Q \leq 0.50$	$0.50 < Q \leq 1.00$
Fire model type	Parametric Fire	ISO834
Quantile Range	$0 < Q \leq 0.50$	$0.50 < Q \leq 1.00$
Thermal Model	Uncertainty	Nominal values
Quantile Range	$0 < Q \leq 0.50$	$0.50 < Q \leq 1.00$

Table 6. Sensitivity indices S_T for the thermal response of unexposed surface

Total Sensitivity Indices S_T	At 20% of t_{max}	At 60% of $_{tmax}$	At 100% of t_{max}
Constitutive models type	0.19	0.45	0.36
Fire model type	0.27	0.77	0.92
Variability in constitutive material model	0.22	0.38	0.32

Table 7. Sensitivity indices S_T for the thermal response of steel rebar

Total Sensitivity Indices S_T	At 20% of t_{max}	At 60% of t_{max}	At 100% of t_{max}
Constitutive models type	0.17	0.05	0.04
Fire model type	0.96	1.27	1.27
Variability in constitutive material model	0.16	0.06	0.05

4.3 Reliability Analysis

As the uncertainty of material and fire scenarios variables was modelled, a reliability analysis can be performed to examine the combined effect of type of material model and its variability. Monte Carlo simulation was used to examine the reliability of RC walls considering the temperature of steel rebars. A value is selected randomly for each input variable based on the developed probabilistic models for fire and material models. The process is repeated, and the probability of exceeding the thermal-failure criteria (temperature of steel rebar exceeds 593°C) was calculated. Then the probability of failure, a conditional probability upon the occurrence of the occupancy-specific fire scenario, was calculated. The gaussianity of the limit state function was tested. It was found that the steel rebar temperatures in normal-strength concrete wall follow a normal distribution, and steel rebar temperatures in high-strength concrete wall follow a lognormal distribution informed by Bayesian Information Criterion (BIC). Fig. 15 compares the cumulative distribution function of the actual data points and the fitted data points to a normal distribution for the temperature of steel rebar in NSC wall and lognormal distribution for the temperature of steel rebar in HSC walls, respectively. Therefore, the reliability indices are calculated using Eq. 6 for NSC wall and Eq. 7 for HSC wall. The calculated reliability indices are conditional upon the occurrence of the occupancy-specific fire scenario used in the analysis. Based on the used limit state, it is found that the reliability index (β) for normal-strength concrete wall is 2.55, which decreased sharply for high-strength concrete to reach 0.611 as spalling occurred in HSC walls. Thus, emphasising the impact of material type and its uncertainty on the thermal performance and, consequently, the reliability of the wall's performance. Furthermore, this stresses the imperative for additional exploration into the impact of fire occurrence rate on the reliability indices when considering the material uncertainty, as it will evaluate the reliability indices employed in the descriptive approaches.

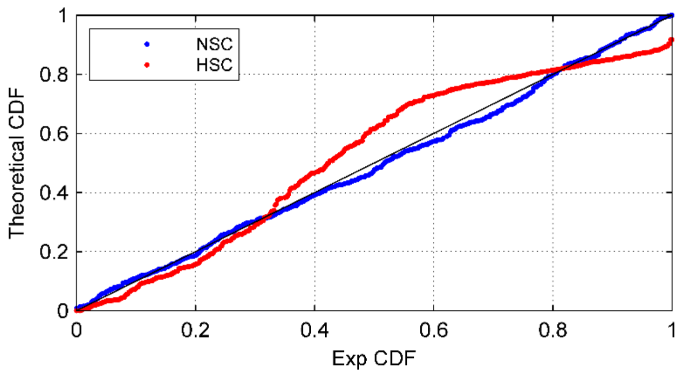

Fig. 15. The probability-probability plot for the temperature of the steel rebar of NSC and HSC walls

5 Conclusions

High-strength and high-performance concrete are increasingly used in the construction industry. A thorough review of open literature and fire guides concludes a wide variability and high uncertainty in the published material models, including the ones for normal-strength concrete. The study examines the effect of material models, normal-strength and high-strength, on the thermal response of reinforced concrete walls. OAT sensitivity analysis was used to quantify the significance of variability in constitutive modelling on the wall's thermal response. Moreover, the study extended the sensitivity analysis to assess the effect of constitutive models, fire models, and variability in constitutive models on the thermal response of reinforced concrete walls. The impact of thermal conductivity variability is influenced by the temperature-dependent rate of decrease in the property and by the scatter of experimental data. The latter is evident for NSC and the former is evident for HSC. Therefore, more testing and improvement in material modelling is needed. Furthermore, the heating rate and fire scenario is the dominant factor in assessing the wall's performance as it is the causal factor to spalling in HSC walls. And finally, the reliability of wall's thermal performance decreased sharply for high-strength concrete due to the spalling of the concrete.

References

Ali, F. (2002), "Is high strength concrete more susceptible to explosive spalling than normal strength concrete in fire?", *Fire and Materials*, Vol. 26 No. 3, pp. 127–130, doi: 10.1002/fam.791.

Andrea Saltelli, Marco Ratto, Terry Andres, Francesca Campolongo, Jessica Cariboni, Debora Gatelli, Michaela Saisana, S.T. (2008), “Sensitivity Analysis: From Theory to Practice”, *Global Sensitivity Analysis. The Primer*, John Wiley & Sons, Ltd, Chichester, UK, pp. 237–275, doi: 10.1002/9780470725184.ch6.

Campolongo, F., Saltelli, A. and Cariboni, J. (2011), “From screening to quantitative sensitivity analysis. A unified approach”, *Computer Physics Communications*, Vol. 182 No. 4, pp. 978–988, doi: 10.1016/j.cpc.2010.12.039.

Castillo, C. and Durrani, A.J. (n.d.). “Effect of Transient High Temperature on High-Strength Concrete”.

Damian, A., Crozier, D.A. and Sanjayan, J.G. (2000), “Tests of Load-Bearing Slender Reinforced Concrete Walls in Fire”, *ACI Structural Journal*, Vol. 97 No. 2.

Eurocode 1. (2005), *Eurocode 1: Actions on Structures - Part 1-4: General Actions.*

Hawileh, R.A. and Kodur, V.K.R. (2018), “Performance of reinforced concrete slabs under hydrocarbon fire exposure”, *Tunnelling and Underground Space Technology*, Vol. 77, pp. 177–187, doi: 10.1016/j.tust.2018.03.024.

Janssens, M. and Dasgupta, B. (2020), “Development and application of a simulation approach for fire and structure interaction of concrete members subject to spalling”, *Fire and Materials*, Vol. 44, John Wiley and Sons Ltd, pp. 365–380, doi: 10.1002/fam.2781.

Karaki, G., Hawileh, R.A. and Kodur, V.K.R. (2021), “Probabilistic-Based Approach for Evaluating the Thermal Response of Concrete Slabs under Fire Loading”, *Journal of Structural Engineering*, Vol. 147 No. 7, p. (ASCE)ST.1943-541X.0003039, doi: 10.1061/(ASCE)ST.1943-541X.0003039.

Karaki, G. and Naser, M.Z. (2022), “An approach for developing probabilistic models for temperature-dependent properties of construction materials from fire tests and small data”, *Fire and Materials*, doi: 10.1002/fam.3116.

Kodur, V. and Mcgrath, R. (2003), “Fire Endurance of High Strength Concrete Columns”, *Fire Technology*, Vol. 39 No. 1, pp. 73–87, doi: 10.1023/A:1021731327822.

Kodur, V.K.R. (2008), “Strategies for improving the performance of high-strength concrete columns under fire hazard”, *Structural Control and Health Monitoring*, Vol. 15 No. 6, pp. 921–938, doi: 10.1002/stc.237.

Mendis, P. (2003), “Design of high-strength concrete members: state-of-the-art”, *Progress in Structural Engineering and Materials*, Vol. 5 No. 1, pp. 1–15, doi: 10.1002/pse.138.

Mueller, K.A. and Kurama, Y.C. (2015), “Out-of-Plane Behavior and Stability of Five Planar Reinforced Concrete Bearing Wall Specimens under Fire”, *ACI Structural Journal*, Vol. 112 No. 6, doi: 10.14359/51687908.

Naus, D. (2010), *A Compilation of Elevated Temperature Concrete Material Property Data and Information for Use in Assessments of Nuclear Power Plant Reinforced Concrete Structures*.

Ngo, T., Fragomeni, S., Mendis, P. and Ta, B. (2013), “Testing of normal-and high-strength concrete walls subjected to both standard and hydrocarbon fires”, *ACI Structural Journal*, Vol. 110 No. 3, pp. 503–510, doi: 10.14359/51685607.

Nguyen, K.T.Q., Ngo, T., Mendis, P. and Heath, D. (2018), “Performance of high-strength concrete walls exposed to fire”, *Advances in Structural Engineering*, SAGE Publications Inc., Vol. 21 No. 8, pp. 1173–1182, doi: 10.1177/1369433217732500.

Novak A. S., C.K.R. (2013), *Reliability of Structures*, 2nd Editio., CRC Press Taylor & Francis Group.

Phan, L.T. (2008), “Pore pressure and explosive spalling in concrete”, *Materials and Structures*, Vol. 41 No. 10, pp. 1623–1632, doi: 10.1617/s11527-008-9353-2.

Phan, L.T. and Carino, N.J. (1998), “Review of Mechanical Properties of HSC at Elevated Temperature”, *Journal of Materials in Civil Engineering*, Vol. 10 No. 1, pp. 58–65, doi: 10.1061/(ASCE)0899-1561(1998)10:1(58).

Sanjayan, J.G. (2011), “Adverse effects in high strength concrete when exposed to fire”, *Concrete in Australia*, Vol. 37 No. 2.